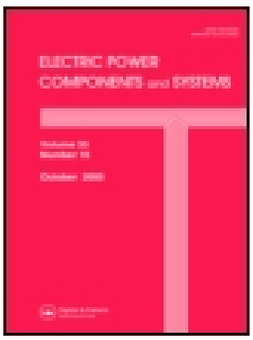

Taylor & Francis
Taylor & Francis Group

Electric Power Components and Systems

ISSN: 1532-5008 (Print) 1532-5016 (Online) Journal homepage: http://www.tandfonline.com/loi/uemp20

Electromagnetic Design and Analysis of a Novel Axial-Transverse Flux Permanent Magnet Synchronous Machine

Mohamed el Hadi Bendib, Mabrouk Hachemi & Fabrizio Marignetti

To cite this article: Mohamed el Hadi Bendib, Mabrouk Hachemi & Fabrizio Marignetti (2017): Electromagnetic Design and Analysis of a Novel Axial-Transverse Flux Permanent Magnet Synchronous Machine, Electric Power Components and Systems, DOI: 10.1080/15325008.2017.1310954

To link to this article: http://dx.doi.org/10.1080/15325008.2017.1310954

Published online: 05 May 2017.

Electric Power Components and Systems, 0(0):1–13, 2017

ISSN: 1532-5008 print / 1532-5016 online
DOI: 10.1080/15325008.2017.1310954

Taylor & Francis
Taylor & Francis Group

Electromagnetic Design and Analysis of a Novel Axial-Transverse Flux Permanent Magnet Synchronous Machine

Mohamed el Hadi Bendib,[1] Mabrouk Hachemi,[1] and Fabrizio Marignetti[2]
[1]Electrical Engineering Department, Laboratoire d'automatique de Sétif-1 (LAS), Ferhat Abbas University, Sétif, Algeria
[2]DIEI, Department of Electrical and Information Engineering, University of Cassino and South Lazio, Cassino (FR), Italy

CONTENTS

Abstract—This paper analyzes a novel hybrid axial-transverse flux permanent magnet (PM) synchronous motor achieving high torque density. The stator pole pitch and the rotor pole pitch are the same. The motor is suitable for vehicle traction systems. The new axial-transverse machine has a single-sided or double-sided air gap. The machine has two adjacent quasi-U stator cores with ring-type winding, and the rotor has two PM groups, one outer and one inner. The shape of quasi-U stator core allows changing the flux path without changing power supply polarity. The analytical expressions of the no-load back-EMF and the torque are derived, after the development of 3-D magnetic equivalent circuit (MEC) model. The 3-D finite element method (FEM) is used to analyze the magnetic field, torque, and cogging torque for different skewings of the PMs.

1. INTRODUCTION

During the last decades, different topologies of Transverse-Flux Permanent Magnet Synchronous Machines (TFPMSMs) have been proposed: the flux constricting TFPMSM [1], surface-mounted permanent magnet (PM) [2], claw-pole TFPMSM [3], single-sided or double-sided TFPMSM [4], C-core, U-core, and E-core stator TFPMSM [5]. The main advantages of TFPMSM are high power density, simple winding, shorter end windings, close-to-unity winding factor, and possibility of modular construction [6].

In TFPMSM with U-type stator cores, the cores of each phase are displaced of twice the pole pitch, and half of the permanent magnets are inactive. Therefore the machine is characterized by a large rotor flux leakage [7, 8]. In fact, in the U-shape TFPMSM, the number of PMs is twice the number of cores.

In the C-type, E-type, and other stator core pieces, the flux direction is the same, and the stator core pieces are spaced twice the pole pitch [9].

This paper presents a novel Axial-Transverse Permanent Magnet Synchronous Machine (A-TFPMSM).The

Keywords: axial flux machine, transverse flux machine, permanent magnets, cogging torque, finite element analysis (FEA), MEC circuit model, reluctance circuit, machine design, synchronous machine, ring winding
Received 27 July 2016; accepted 6 March 2017
Address correspondence to Fabrizio Marignetti, DIEI, Department of Electrical and Information Engineering, University of Cassino and South Lazio, via G.Di Biasio 43, Cassino (FR) 03043, Italy. E-mail: marignetti@unicas.it
Color versions of one or more of the figures in the article can be found online at www.tandfonline.com/uemp.

A-TFPMSM has two configuration possibilities, the first has all three-phase coil windings arranged on one side and the second has each phase coil wound on each side. In the first configuration, the stator cores pitch is not equal to the magnet rotor poles pitch, significantly increasing the leakage [10] between the magnetic poles, and decreasing the flux linkage.

The disadvantage of the single-sided A-TFPMSM can be compensated by using the second configuration. This configuration leads to the multi-disc or multi-stage A-TFPMSM model proposed in this paper. In this configuration, the stator core pitch and the rotor magnet pole pitch are equal, maximizing the torque density and the flux linkage, and obviously minimizing the leakage flux.

Furthermore, A-TFPMSM stator cores can use steel laminations, because the path of magnetic flux lines is two dimensional. Iron core loss is reduced in this way while the magnetic flux density is increased.

The A-TFPMSMs are suitable for a slim shape with a relatively short axial length and have a limitation on the increase in power for a given outer diameter of the machine [11].

The magnetic equivalent circuit (MEC) method has been chosen in electrical machine study, and is very useful for the design of different types of electrical machine, including linear machines [12], AFPM machines [13], and TFPM machines [14]. A simple and accurate MEC method of the novel A-TFPMSM is adopted. A 3-D MEC model for this type machine has been chosen.

Cogging torque of axial TFPMSM is also an important subject. TFPMSM usually has higher cogging torque, when compared to other types of PM machines, due to the large number of rotor poles [15]. The methods described in the literature for reducing the cogging torque include skewing the magnets of the rotor or the stator poles [16].

This paper presents a novel axial flux-concentrated TFPMSM with new rotor and stator structures. A 3-D representation of the quasi-U stator core A-TFPMSM is shown in Figure 1. To validate the proposed design, the 3-D finite element analysis simulation is used.

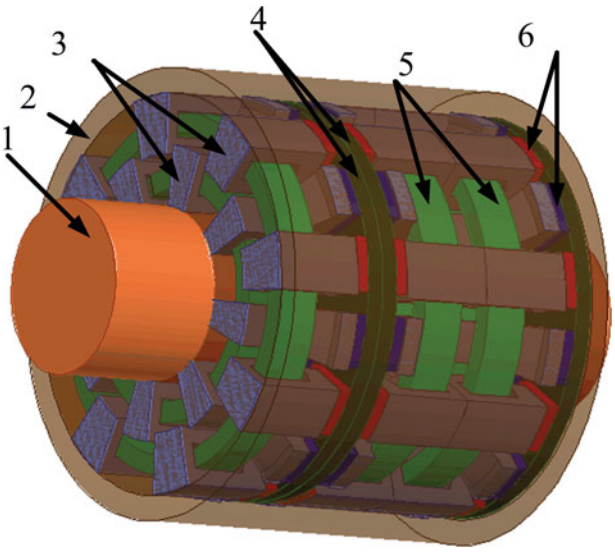

FIGURE 1. Structure of A-TFPMSM. (1) Shaft, (2) housing, (3) stator cores, (4) rotor, (5) coils, and (6) permanent magnets.

2. MACHINE STRUCTURE AND PRINCIPLE OF OPERATION

2.1. Machine Topologies

Figure 1 shows the basic structure of the A-TFPMSM, which consists of one rotor core, one stator core, windings, and PMs.

The stator winding of A-TFPMSM features a modular structure and can be arranged as needed. The stator winding can be arranged into three phases for both the one-sided (Figure 2(b)) and the double-sided machine (Figure 2(a)); or into one phase for both the one-sided machine (Figure 2(d)), and the multi-sided machine (Figure 2(c)). In the embodiments of Figure 2a and Figure 2b, each phase coil occupies one third of the stator core.

In Figure 2b, the stator winding form is a ring portion. This configuration has two disadvantages: the one is the presence of the end connections and the second is that the pole pitches of the stator and the rotor are different. Also, unbalanced

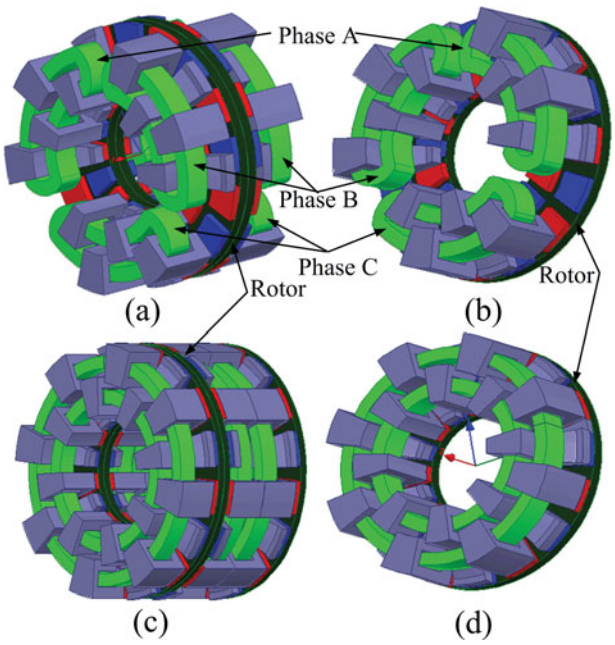

FIGURE 2. Different configurations of the A-TFPMSM.

pulling forces arise as the currents in the three phases are not instantaneously the same. The main advantage of this configuration is that it can be used either in the single-side or in the multiple-side layouts.

In Figure 2d, the two main disadvantages of the first design (Figure 2b) are overcome; by using the ring winding, there are no end windings and the pole pitch of the stator and the rotor are the same. However, the simple one-sided construction is impossible. The proposed configuration is thus that of Figure 2(c).

Figure 2(c) and (d) show that the structure of A-TFPMSM has a three-phase ring winding, with each phase occupying one stator side. The machine can be built with multi-sided stator also. This configuration, which is shown in Figure 2(c), is even more advantageous and will be dealt with in this paper.

2.2. A-TFPMS Machine Principle

The cross-sectional view of the machine in Figure 3 shows the magnetic flux path. Two quasi-U cores are traversed by fluxes going in opposite directions. The proposed position of the stator core is very important, because the change of the direction of magnetic flux path is necessary to keep the torque orientation. Two PMs are in the inner and outer radii, and magnetized in opposite direction, generating the flux in opposite directions for two consecutive poles.

The windings are supplied by an alternating power, creating the magnetic flux in the stator. The stator flux interacts with the rotor PM field, which produces the force that rotates the machine.

3. MAGNETIC CIRCUIT CALCULATION

As shown in Figure 3, the flux paths cutting the air gap of this machine have two loops; one is represented by the flux line crossing the rotor PMs (*i.e.* both the outer and the inner PMs). This loop contains the flux in the radial (normal) direction. The second loop is represented by the flux line crossing the rotor through adjacent PMs poles (four PMs), this loop has two tangential flux lines.

In Figure 4, we converted the 3D MEC to an equivalent 2D MEC to achieve simplified Kirchhoff's loop equations.

The basic equations for each element of the equivalent magnetic circuit loop in Figure 4 are as follows:

1- By using Kirchhoff's law, the flux equations in the different parts of the machine are:

$$\begin{aligned} \Phi_{gap} &= \Phi_{PM2} - \Phi_{Ln} - \Phi_{Lt2} \\ \Phi_{PM1} &= \Phi_{rt2} + \Phi_{rn} \\ \Phi_{PM2} &= \Phi_{rt1} + \Phi_{rn} \end{aligned} \tag{1}$$

where Φ_{gap} is the main magnetic flux, Φ_{PM1} and Φ_{PM2} are the permanent magnet flux, Φ_{Lt2} and Φ_{Ln} are the air-gap flux leakage in the tangential and normal directions, respectively, and Φ_{rt1}, Φ_{rt2}, and Φ_{rn} are the fluxes in the rotor in the tangential and normal directions, respectively.

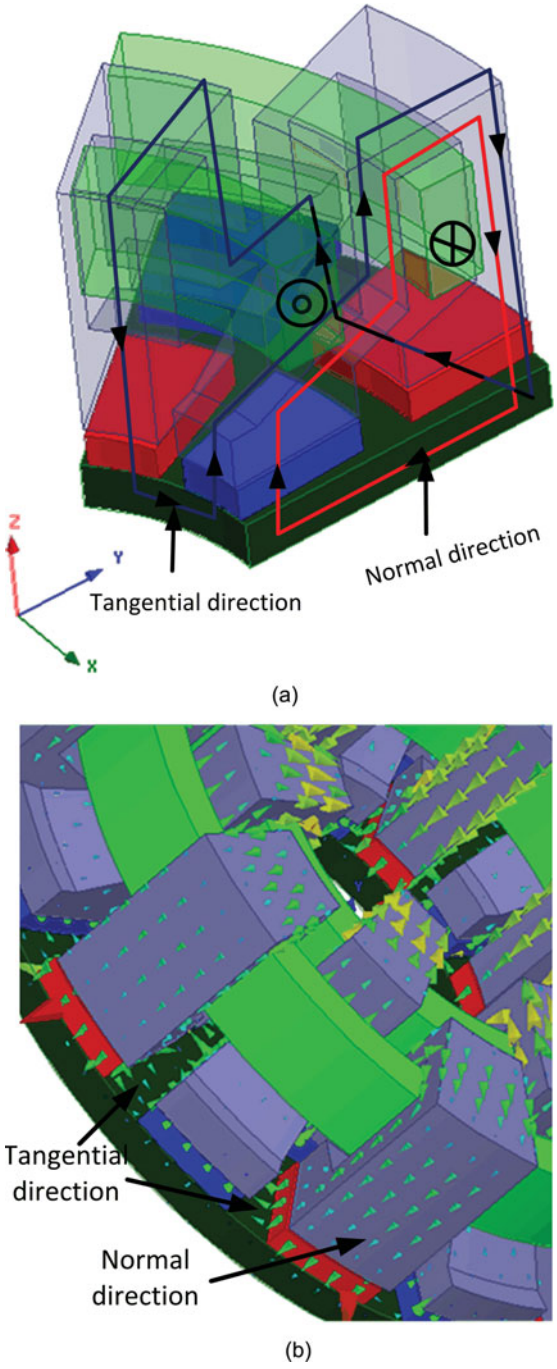

FIGURE 3. Flux path in two pole pairs of A-TFPMSM for single-sided and one phase.

2- The *MMF* equations achieved by using Ohm's law for magnetic circuits yields:

$$\begin{aligned} 0 &= 2\Phi_{Ln}R_{Ln} - \Phi_{Lt1}R_{Lt1} - \Phi_{Lt2}R_{Lt2} \\ 0 &= 2\Phi_{rn}R_{rn} - \Phi_{rt1}R_{rt1} - \Phi_{rt2}R_{rt2} \end{aligned}$$

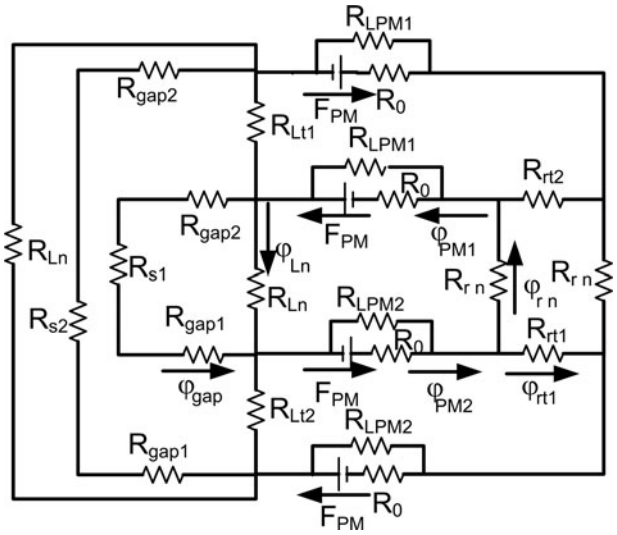

FIGURE 4. A-TFPMSM simplifies equivalent magnetic circuit.

Quantity	Value
Output power	2 KW
Input voltage	220 V
Speed	375 rpm
Self-inductance	18.56 mH
Coercive field magnets	900 KA/m
Peak current	10 A
Remanence flux density of PM	1.3 T
Wire current density	4 A/mm^2
Frequency	100 Hz
Air gap	0.5 mm
Magnet type	NdFeB
Power factor	0.708
Current loading density	19 KA/m
Poles numbers	32
Number of windings turns	120
Iron core type	Steel 1008

TABLE 1. Specifications of the designed A-TFPMSM

$$0 = \Phi_{Ln}R_{Ln} - \Phi_{gap}\left(R_{s1} + R_{gap}\right) \tag{2}$$

where the reluctances R_{Ln} and R_{Lt1} and R_{Lt2} are the air-gap leakage reluctances in the normal and tangential direction, respectively. R_{rn} and R_{rt1} and R_{rt2} are the rotor core reluctances in the normal and the tangential direction, respectively. Finally, R_{s1} and R_{s2} are the reluctances of the inner and outer stator cores. R_{gap} is the air-gap reluctance, where $R_{gap} = R_{gap1} + R_{gap2}$

3- The *MMF* of the PM is dehfined as:

$$F_{PM} = \frac{B_r h_{PM}}{\mu_{rm}\mu_0} \tag{3}$$

where μ_0, μ_{rm}, B_r, and h_{PM} are the air permeability, the recoil permeability, the remanence, and the length of the PM in z-axis direction, respectively.

$$\begin{aligned} F_{PM} &= \left(2\Phi_{PM2}R_{eq2} + \Phi_{Lt2}R_{Lt2} + \Phi_{rt1}R_{rt1}\right)/2 \\ F_{PM} &= \left(2\Phi_{PM1}R_{eq1} + \Phi_{Lt1}R_{Lt1} + \Phi_{rt2}R_{rt2}\right)/2 \\ 2F_{PM} &= \left(\Phi_{PM1}R_{eq1} + \Phi_{PM2}R_{eq2} + \Phi_{Ln}R_{Ln} + \Phi_{rn}R_{rn}\right) \\ 2F_{PM} &= \left(\Phi_{PM1}R_{eq1} + \Phi_{PM2}R_{eq2} + \Phi_{gap}(R_{gap} + R_{s2}) + \Phi_{rn}R_{rn}\right) \end{aligned} \tag{4}$$

where R_{eq1} and R_{eq1} are the PM leakages equivalents reluctances.

The PM leakage equivalent reluctance can be written as:

$$\begin{aligned} R_{eq1} &= R_{LPM1}//R_{01} = R_{LPM1}R_{01}/(R_{LPM1} + R_{01}) \\ R_{eq2} &= R_{LPM2}//R_{02} = R_{LPM2}R_{02}/(R_{LPM2} + R_{02}) \end{aligned} \tag{5}$$

where R_{01} and R_{02} are the PM reluctance, R_{LPM1} and R_{LPM2} are the PM leakages reluctances.

Solving equation (4) and introducing the expressions of the equivalent reluctances (5), the main flux is achieved as:

$$\Phi_{gap} = \frac{2F_{PM}\left(R_{10}R_{12} - R_{13}R_{11}\right)}{R_{10}R_{14} - R_{13}R_9} \tag{6}$$

where R_9, R_{10}, R_{11}, R_{12}, R_{13}, and R_{14} are provided in Appendix II.

Figure 4 presents the MEC of two neighboring poles. As the geometry of stator cores are different, the two reluctances R_{s1} and R_{s2} are different. The machine air gap also has two sections: the first is the outer section and the second is the inner. For this reason, even the two air-gap reluctances R_{gap1} and R_{gap2} are different. Similarly, the PM dimensions are different (as the outer section is larger than the inner section). This implicates that the reluctances R_{01} and R_{02} are different. The rotor has four reluctance values; the radial or normal reluctances R_{rn} are equal while the tangential reluctances R_{rt1} and R_{rt2} are different (Table 2).

The reluctances of the PMs R_{01} and R_{02} are defined as:

$$R_{01} = \frac{h_{PM}}{\mu_{rm}\mu_0 S_{PM1}} \quad R_{02} = \frac{h_{PM}}{\mu_{rm}\mu_0 S_{PM2}} \tag{7}$$

where S_{PM1} and S_{PM2} are the sections of the PMs.

The air-gap reluctance R_{gap} is a function of the rotor position, which can be obtained as:

$$R_{gap} = \frac{1}{\mu_0 h_{PM}} \int_0^{h_{PM}} \frac{g(z)}{dz} \tag{8}$$

where $g(z)$ is the function representing the air-gap length.

The values of all reluctances of the proposed MEC of one A-TFPMSM design are provided in the Appendix 1.

Parameter	Value (mm)
PM thickness	$h_{PM} = 6$
PM length	$l_{PM} = 15$
Width of stator coil	$b_s = 15$
Width of stator core	$b_{st} = 10$
Hight of stator	$h_s = 56$
Hight of stator yoke	$h_{sy} = 8$
Hight of stator coil	$h_{s1} = 32$
Hight of stator shoe	$h_{st} = 11$
Hight of rotor	$h_r = 10$
Width of stator shoe	$w_{st} = 27$
Inner diameter	$R_i = 50$
Outer diameter	$R_o = 95$
Pole pitch	37.3
Pole arc coefficient	0.80

TABLE 2. Geometric parameters of the designed A-TFPMSM

The self-inductance of each phase winding can be computed from the integral of the energy stored in the magnetic field when a given current source is applied to the windings and no magnets are present. The energy integral must be computed in several domains, namely back iron, air gap, slots, and end turns. In the proposed machine, there is no end-turn inductance and it is even possible to neglect the back-iron inductance. Therefore, the phase inductance of the stator winding can be computed from the sum of the air gap and of the slot leakage reactances as [11, 22, 23]:

$$L_{g1,2} = \frac{pN_{ph}^2}{2\left(R_{g1,2} + R_{01,2}\right)} \tag{9}$$

$$L_s = \mu_0 \pi N_{ph}^2 \left((2R_o - b_{st} - b_s) \cdot \left(\lambda_{ls} + \lambda_{lp}\right)\right) \tag{10}$$

where p is the number of pole pairs, λ_{ls} and λ_{lp} are the coefficients of the slot permeance and pole-top leakage permeance, respectively, and the meanings of the other symbols are given in Appendix 1.

4. SOLVING METHOD

To validate the method, a MEC has been established, and the resulting circuit is shown in Figure 4 where the main and leakage flux paths are shown by arrows.

The determination of each flux is achieved through Hopkinson's Law, which is expressed as follows:

$$F = R\Phi \tag{12}$$

where R, F, and Φ are matrix reluctance, MMF, and flux, respectively.

Knowing the number of the nodes and the loops of the circuit in Figure 4, we will determine the numbers of independent loops that are set up in matrix form.

The MMF flux law can be derived as follows:

The reluctance matrix is a diagonal square matrix composed of the reluctances of different branches of the circuit with dimensions of 14* 14. The matrix of the MMF is a matrix of m* 1 with $m = 7$, the number of independent loops of the circuit. The matrix of flux is a matrix of n* 1 dimension with $n = 14$, the number of legs.

To solve the above equation, we use the matrix form

$$\Phi = S^T \left(SRS^T\right)^{-1} F \tag{13}$$

where S is the connectivity matrix, enabling a matrix representation of Kirchhoff's laws. This matrix has m rows and n columns.

To solve MEC model, a numerical procedure is developed. Both the position and the reluctance are varying, as shown in the flowchart given in Figure 5.

As shown in Figure 5, the solution of the MEC starts from the geometrical and material datan, including the relative permeability. Based on these parameters, the reluctances are computed. By using Eq. (13), the flux is achieved. Then the

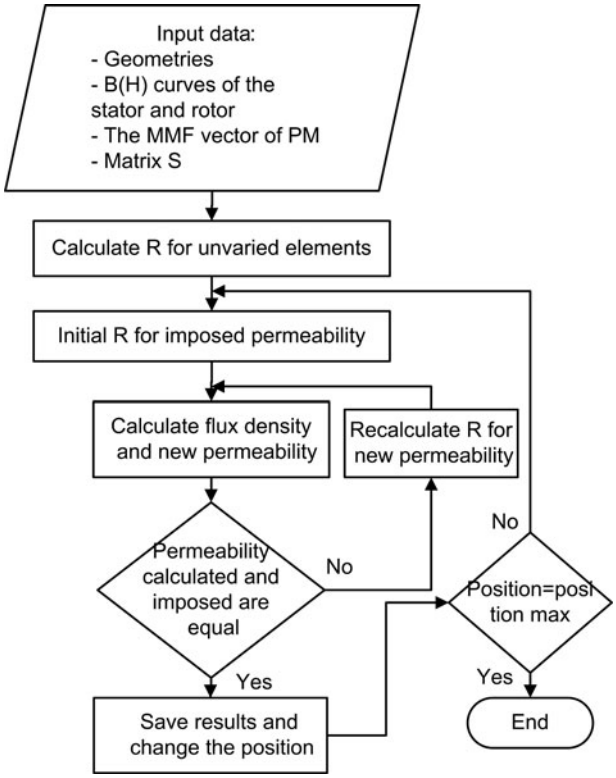

FIGURE 5. Flowchart of procedure used for solving the MEC model.

relative permeability is computed again by using the B(H) curves. The Φ_{gap} results in the previous process are used in the next steps to compute both the EMF and the torque.

5. TORQUE ANALYSIS

The maximum no load flux is achieved when the rotor magnets and the stator cores are aligned. Accordingly, this position will be taken as the initial position for the analysis. According to the rotor position, the air gap can be expressed as:

$$\varphi = k_f \Phi_{gap} \cos \omega t \tag{14}$$

where K_f is the air-gap flux waveform coefficient and Φ_{gap} is the maximum value of the no-load flux.

The flux coefficient in Eq. (14) can be achieved as [22]:

$$k_f = \frac{8}{\pi} \sin \frac{\alpha \pi}{2} \tag{15}$$

where α is the pole arc coefficient in the rotational direction.

By using Faraday's law, the no-load-induced electromotive force can be expressed as

$$e = -N_{ph} \frac{d\varphi}{dt} = 2\pi k_f f N_{ph} \Phi_{gap} \sin(\omega t) \tag{16}$$

where N_{ph} is the number of windings turns and ω is the electrical angular frequency.

The no-load RMS electromotive force EMF of each phase is

$$E = \sqrt{2}\pi k_f f N_{ph} \Phi_{gap} \tag{17}$$

The no-load EMF E in Eq.(17) is proportional to the frequency f and the number of windings turns N_{ph}.

Supplying the windings by three-phase alternating power, the rotor PMs interact with the armature field.

If the space vector of the current is aligned to the q-axis direction, the phase current I_a is in phase with the induced EMF; therefore, assuming a sinusoidal distribution of currents and voltages, it is possible to calculate the power factor as [22]:

$$\cos \varphi \approx \frac{E + RI}{V} \tag{18}$$

The stator current applied is

$$i_a = \sqrt{2} I_a \sin \omega t \tag{19}$$

where I_a is the RMS of the stator current.

The generated electromagnetic power of A-TFPMSM is

$$P_{elem} = m\sqrt{2}2\pi k_f f N_{ph} \Phi_{gap1} I_a \left(\frac{1 - \cos 2\omega t}{2} \right) \tag{20}$$

where Φ_{gap1} is the fundamental main flux calculated in (6), p is the number of pole pairs, and m is the number of phases.

The torque can be obtained by

$$T = \frac{P_{elem}}{2\pi n} = \sqrt{2} m p N_{ph} \Phi_{gap1} I_a \left(\frac{1 - \cos 2\omega t}{2} \right) \tag{21}$$

From Eq. (21) the torque of one phaseof A-TFPMSM is sinusoidal. The torque waveform has two peaks, and the average torque is different from zero.

The electromagnetic torque peak for one phase is

$$T_{\max} = \frac{1}{2} \sqrt{2} m p N_{ph} \Phi_{gap1} I_a \tag{22}$$

The angle between the phase currents is $2\pi/3$; the three-phase torques T_A, T_B, and T_C can be written as follows:

$$\begin{cases} T_A = \sqrt{2} m p N_{ph} \Phi_{gap1} I_a \frac{1}{2} (1 - \cos 2\omega t) \\ T_B = \sqrt{2} m p N_{ph} \Phi_{gap1} I_a \frac{1}{2} \left(1 - \cos(2\omega t - \frac{2\pi}{3})\right) \\ T_C = \sqrt{2} m p N_{ph} \Phi_{gap1} I_a \frac{1}{2} \left(1 - \cos(2\omega t + \frac{2\pi}{3})\right) \end{cases} \tag{23}$$

The total torque is the sum of the all torques generated by the three-phase power supply, that is

$$T = T_A + T_B + T_c = \frac{3}{2} \sqrt{2} m p N_{ph} \Phi_{gap1} I_a \tag{24}$$

6. 3-D FINITE ELEMENTS AND MEC RESULTS

According to the equations listed above, to obtain accurate design results, finite element analysis is necessary. The traditional 2-D model is unsuitable for an accurate simulation as the magnetic flux leakage of A-TFPMSM between adjacent poles is significant [17]. A 3-D finite element analysis is therefore necessary to analyze the magnetic field distribution of the machine, the torque, and the cogging torque.

Stepwise 3-D FE simulation was used to minimize the cogging torque. Each simulation is performed with a different skewing angle of the permanents magnets [18].

The main dimensions of the A-TFPMSM prototype are shown in Table 1.

In Figure 6, the stator has three core unit groups; every unit has its magnetic flux state. In state one Figure 6(a), the stator core unit is aligned to the closest rotor poles. In this case, the stator core flux density is 1 T and the air-gap flux density is 0.78 T. In state two Figure 6(c), the stator core unit is nearly aligned to the rotor poles and the flux lines generated by the PMs cross the air gap. In this case, the stator core flux density is 0.6 T. In state three Figure 6(b), the stator core unit is located between two rotor poles and the flux line generated by the PM cross the air gap. In this case, the stator core flux density is 0.35 T. The magnetic conditions of the A-TFPMSM prototype are acceptable, showing no significant saturation area in the design.

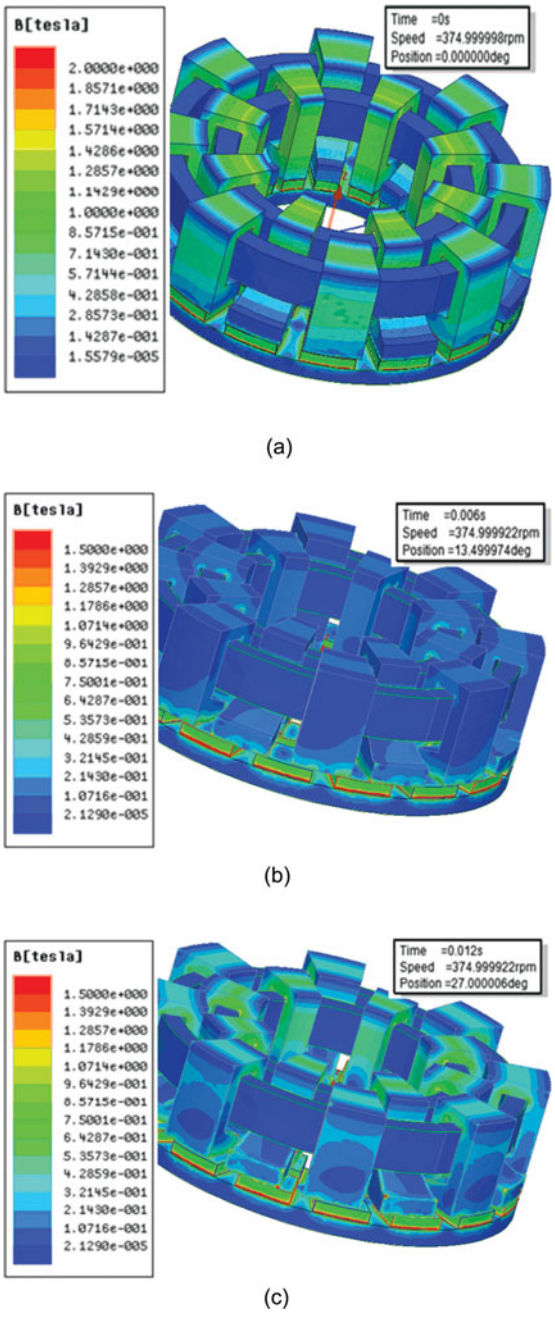

FIGURE 6. Flux density distribution of A-TFPMSM: (a) Stator core aligned to the magnetic poles, (b) stator core between two poles, and (c) stator core nearly almost opposite to the magnet poles.

The computations of the air-gap flux density by using FEA and MEC are shown in Figure 7, where a good agreement is achieved for both results.

The no-load back EMF of the machine at 375 r/min rotation speed for both analyses are shown in Figure 8. By using Eq (14), the EMF RMS is E = 140 V. The waveform of FEA

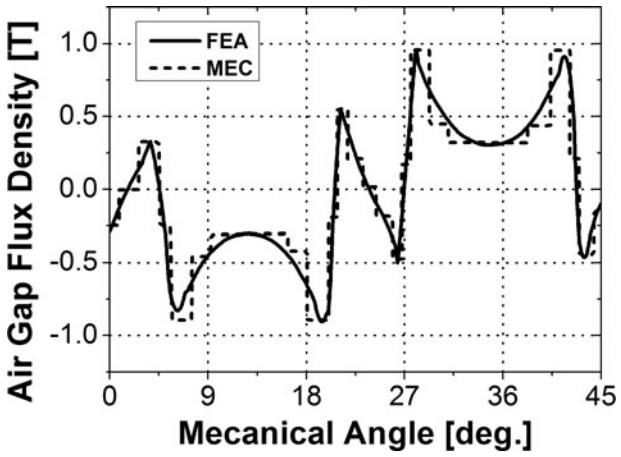

FIGURE 7. Air-gap flux density distribution.

is lower than the waveform of MEC, as the MEC analysis inevitably neglects some of the leakage flux lines The flux linkages at no-load for different positions achieved from both MEC and FEA analyses are shown in Figure 9. The flux linkage is larger at 0 ms when the stator core and PM pole are fully opposite; the flux linkage is smallest at 6 ms when the stator core unit located between two poles. Another important comparison between the first design (shown in Figure a) and the final design (shown in Figure c) is based on the flux linkage, as shown in Figure 14. The flux linkage in the configuration with one phase per each side is larger than the flux linkage in the configuration with three phases per each side. The final design has full pitch and no end winding in comparison to the first design.

In Figure 10, the torques generated by FEA and MEC at different current values and in the position where the stator core are fully aligned to the rotor pole, calculated by using

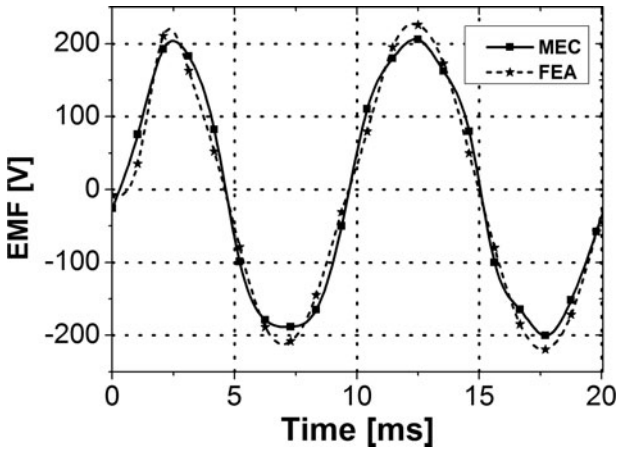

FIGURE 8. No-load back EMF of A-TFPMSM for FEA and MEC.

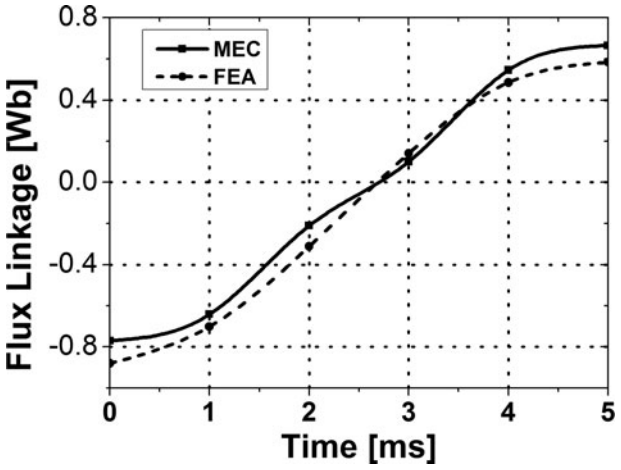

FIGURE 9. Flux linkage at no-load by FEA and MEC.

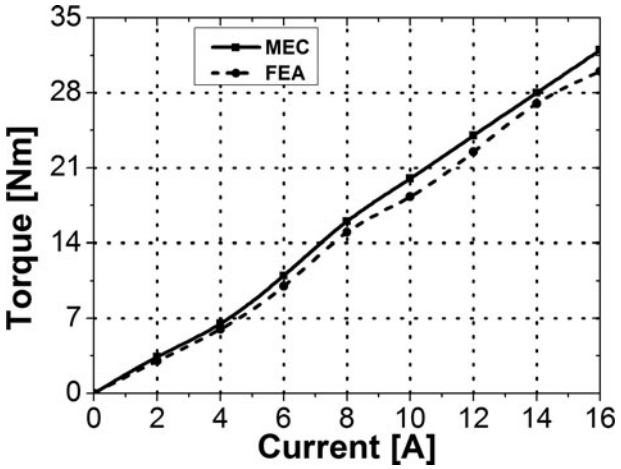

FIGURE 10. Average torque with stator current of A-TFPMSM.

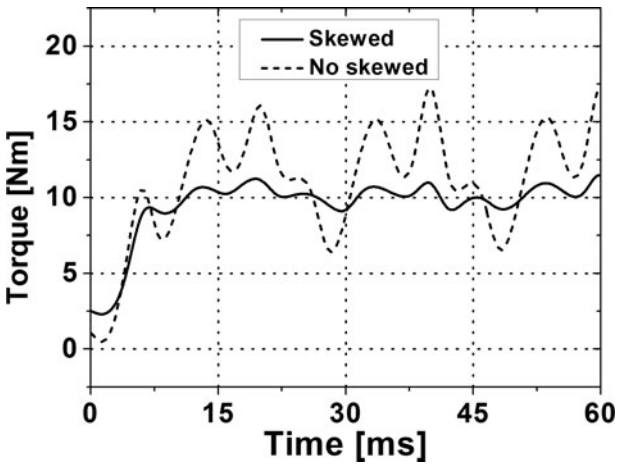

FIGURE 11. Torque generated from FEA transient simulation.

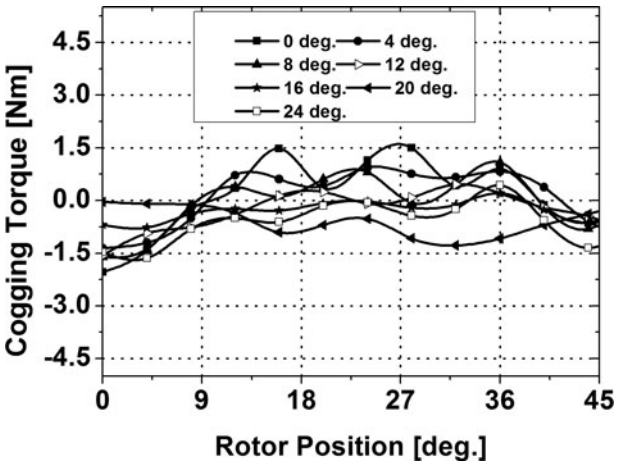

FIGURE 12. Cogging torque for various skews angles.

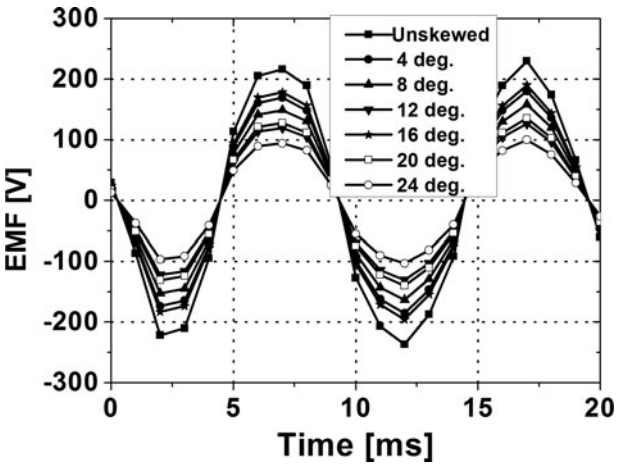

FIGURE 13. Back-EMF waveforms.

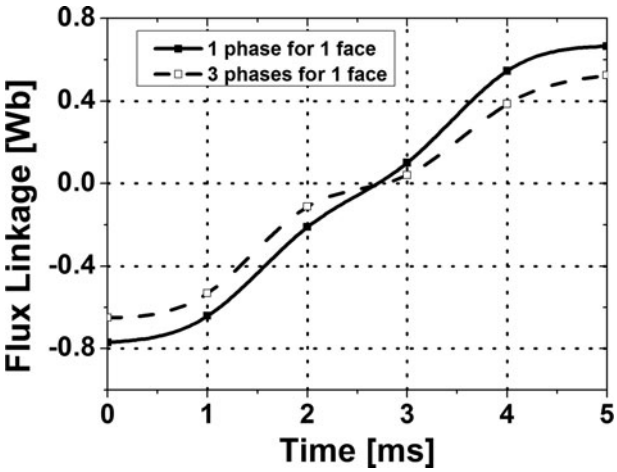

FIGURE 14. Flux linkages of first and final designs.

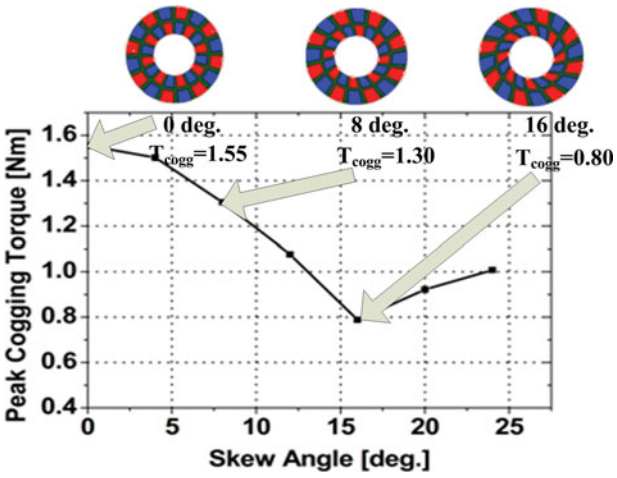

FIGURE 15. Peak cogging torque against skew angles.

Eq. (23), are shown; the results of the proposed method are in good accordance with the FEA simulation.

The torque equation developed in the previous section is used to perform the analysis of the machine torque. The validation of the model is made on the basis of the results obtained from the 3-D transient FEM simulation. The waveform of the generator torque is shown in Figure 11. This waveform has significant oscillations. The cause of this behavior is the cogging torque generated by the air-gap reluctance variation. In order to reduce the cogging torque, we use the PM skewing method. The torque generated after a skewing of PM is shown in Figure 11, where the amplitude of cogging is significantly reduced. The torque of the machine with skewed PMs is less than the machine with no skewing.

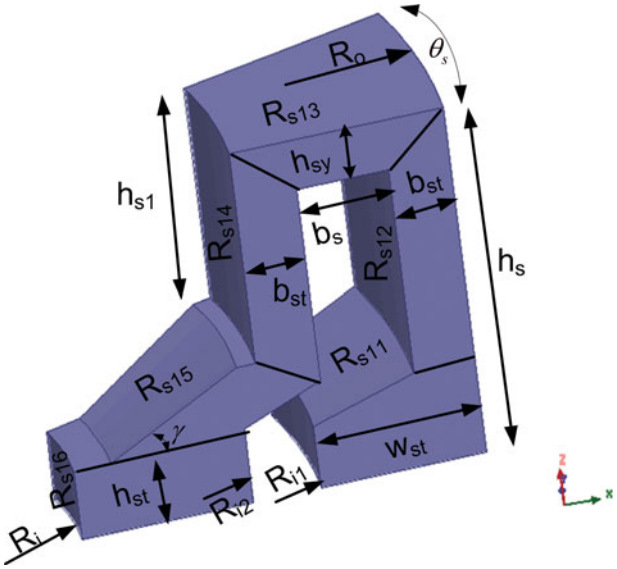

FIGURE 16. Dimensions of the first stator element.

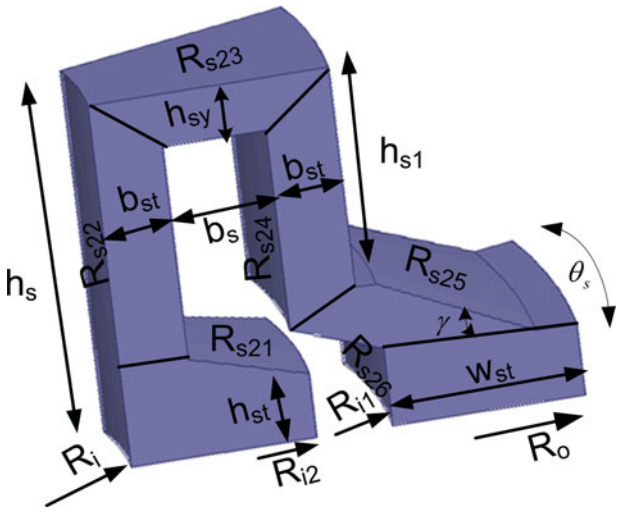

FIGURE 17. Dimensions of the second stator element.

The cogging torque components are shown in Figure 12. Cogging torque is one of the most important sources of torque oscillation [19, 20]. Pole shifting and skewing are the main methods to reduce the cogging torque [20, 21]. The simplest method is skewing the magnets. To find the optimum skew angle of A-TFPMSM, a 3-D FEM analysis for seven different skew angles is used.

The back-EMF waveforms of skewed PM rotor are shown in Figure 13. When the PM core is skewed too deeply, the amplitude of back-EMF declines sharply. The FEM simulation is run for the skew magnet angles 0, 4, 8, 12, 16, 20, and

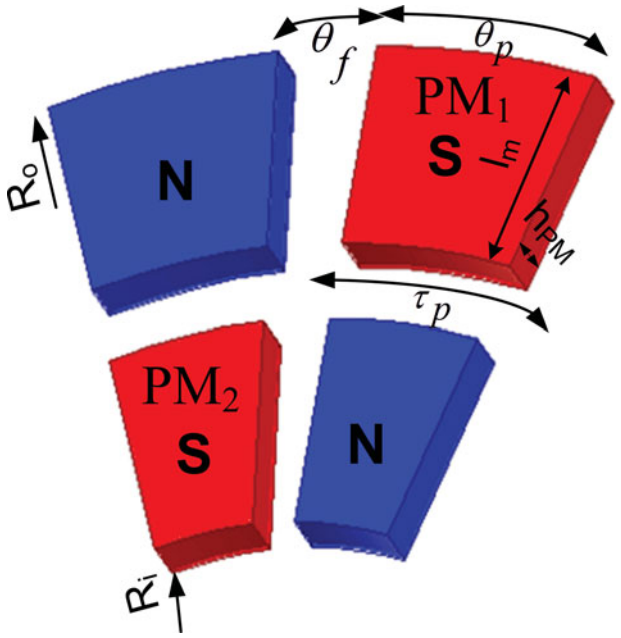

FIGURE 18. Dimensions of permanents magnets.

24°. The results of the simulation are in Figure 12. The peak-to-peak values of the cogging torque are shown in Figure 13. The no-skew cogging torque is 1.55 Nm, while at 16° skew, the minimum cogging torque of 0.8 Nm is achieved. Further increasing the skew angle, the cogging torque starts to increase.

7. CONCLUSION

This paper presents the design of an A-TFPMSM. The quasi-U stator core is very useful for this type of machine, as that core is easy to be manufactured and each of the three phase windings contributes separately to the generation of the electromagnetic torque. The analysis of the torque and the back-EMF is developed.

The developed MEC of novel A-TFPMSM has been used for the analyses of the air-gap flux density, the no-load back EMF, and the flux linkage. To validate the analysis, a 3-D FEM simulation is used.

The 3-D finite element analysis of the axial-transverse flux machine provides the magnetic flux density values in the different sections of machine at no-load. The flux density values are within the standard intervals used for the design of classical machines.

The optimization of the cogging torque has been studied, and the magnet skew method is suggested to reduce the cogging torque.

REFERENCES

[1] Hosseini, S., Moghani, J. S., Ershad, N. F., and Jensen, B. B., "Design, Prototyping, and Analysis of a Novel Modular Permanent-Magnet Transverse Flux Disk Generator," *IEEE Trans. Magn.*, Vol. 47, No. 4, April 2011.

[2] Lee, J.-Y., Hong, D.-K., Woo, B.-C., Park, D.-H., and Nam, B.-U., "Performance comparison of longitudinal flux and transverse flux permanent magnet machines for turret applications with large diameter," *IEEE Trans. Magn.*, Vol. 48, No. 2, pp. 915–918, February. 2012.

[3] Hsu, Y.-S. and Tsai, M.-C., "Development of a novel transverse flux wheel motor," *IEEE Trans. Magn.*, Vol. 47, No. 10, pp. 3677–3680, October 2011.

[4] Jia, Z., Lin, H., Fang, S., and Huang, Y., "A novel transverse flux permanent magnet generator with double c-hoop stator and flux concentrated rotor", *IEEE Trans. Magn.*, March 2015.

[5] Polinder, H., Mecrow, B. C., Jack, A. G., Dickinson, P. G., and Mueller, M. A., "Conventional and TFPM linear generators for direct-drive wave energy conversion," *IEEE Trans. Energy Conv.*, Vol. 20, No. 2, pp. 260–267, June 2005.

[6] J. F.Gieras, and Wing, M.. *Permanent Magnet Motor Technology*. Hndqurncn Marccl Dckker. Inc, 2002.

[7] Wang, J., Howe, D., and Lin, Z., "Design optimization of short-stroke single-phase tubular permanent-magnet motor for refrigeration applications,"*IEEE Trans. Ind. Electron.*, Vol. 57, No. 1, pp. 327–334, January 2010.

[8] Zou, J., Q.Wang, and Xu, Y., "Influence of permanent magnet magnetization length on the performance of a tubular transverse flux permanent magnet linear machine used for electromagnetic launch," *IEEE Trans.Plasma Sci.*, Vol. 39, No. 1, pp. 241–246, January 2011.

[9] Yang, G., Cheng, D., Zhang, H., and Kou, B., "Bidirectional cross-linking transverse flux permanent magnet synchronous motor" *IEEE Trans. Magn.*, Vol. 49, No. 3, March 2013.

[10] Lu, K., Rasmussen, P. O., and Ritchie, E., "Design considerations of permanent magnet transverse flux machines," *IEEE Trans. Magn.*, Vol. 47, No. 10, pp. 2804–2807, October 2011.

[11] Gieras, J. F., Wang, R. J., and Kamper, M. J.. *Axial Flux Permanent Magnet Brushless Machines*. Kluwer Academic Publishers, 2004.

[12] Souissi, A., Zouaghi, M. W., Abdennadher, I., and Masmoudi, A.,"MEC-based modelling and sizing ofa tubular linear PM synchronous machine," *IEEE Trans. Ind. Appl.*, Vol. 51, No. 3, pp. 2181–2194, 2015.

[13] Maloberti, O., Figueredo, R., Marchand, C., Choua, Y., De Condamin, , Kobylanski, L., and Bommé, E., "3-D–2-D Dynamic magnetic modeling of an axial flux permanent magnet motor with soft magnetic composites for hybrid electric vehicles," *IEEE Trans. Magn.*, Vol. 50, No. 6, 2014.

[14] Hosseini, S., Shokrollahi Moghani, J., Ershad, N. F., and Jensen, B. B., "Design, prototyping, and analysis of a novel modular permanent-magnet transverse flux disk generator," *IEEE Trans. Magn.*, Vol. 47, No. 4, April 2011.

[15] Dobzhanskyi, O., and Gouws, R., "Performance analysis of a permanent magnet transverse flux generator with double coil," *IEEE Trans. Magn.*, Vol. 52, No. 1, January 2016.

[16] Ahn, H., Jang, G., Chang, J., Chung, S., and Kang, D., "Reduction of the torque ripple and magnetic force of a rotatory two-phase transverse flux machine using herringbone teeth," *IEEE Trans. Magn.*, Vol. 44, No. 11, November 2008.

[17] Schmidt, E., "Finite element analysis of a novel design of a three phase transverse flux machine with an external rotor," *IEEE Trans. Magn.*, Vol. 47, No. 5, May 2011.

[18] *Maxwell 3D V16 User's Guide*. Maxwell Online Help Ansys Inc., 2010.

[19] Bianchi, N. and Bolognani, S., "Design techniques for reducing the cogging torque in surface-mounted PM motors," *IEEE Trans. Ind. Appl.*, Vol. 38, No. 5, pp. 1259–1265, September/October 2002.

[20] Aydin, M., "Effects of magnet skew in cogging torque minimization ofaxial gap permanent magnet motors," in *Proc. 18th ICEM*, Villamoura, Portugal, 2008.

[21] Aydin, M., Huang, S., and Lipo, T. A., "Design, analysis, and control of a hybridfield-controlled axial-flux permanent-magnet motor" *IEEE Trans. Iind. Elec.*, Vol. 57, No. 1, January 2010.

[22] Gieras, J. F., Wing, M. *Permanent Magnet Motor Technologie Design and Application*. Marccl Dckker, New York, 2002.

[23] Hanselman, D. C.. *Brushless Permanent Magnet Motor Design*. McGraw-Hill, Inc., New York, 1994.

APPENDIX 1

Magnetic Equivalent Circuit Reluctances

In Figures 16 and 17, the geometry of stator cores is shown. Each portion has its own section area S and length l that differ from the others.

(1) Reluctance of the first stator element: R_{S1}

The total reluctance of the first stator element is the sum of all stator portions as follows:

$$R_{S1} = R_{S11} + R_{S13} + R_{S14} + R_{S15} + R_{S16} \tag{A.1.1}$$

■ *Length and surface RS_{11}*

$$R_{S11} = \frac{l_{S11}}{\mu_0 \mu_{r11}(B) S_{S11}} \tag{A.1.2}$$

where

$$l_{S11} = h_{ST} \tag{A.1.3}$$

$$S_{S11} = \frac{2\pi}{P}\alpha\left(R_o^2 - (R_o - w_{st})^2\right) \tag{A.1.4}$$

■ *Length and surface RS_{12}*

$$l_{S12} = h_s - h_{st} - hsy_{/2} \tag{A.1.5}$$

$$S_{S12} = \frac{2\pi}{p}\alpha\left(R_o^2 - (R_o - B_{st})^2\right) \tag{A.1.6}$$

■ *Length and surface RS_{13}*

$$l_{S13} = b_s + b_{st} \tag{A.1.7}$$

$$S_{S13} = \frac{2\pi}{p}\alpha\frac{h_{sy}(b_s + b_{st})}{\ln\left(\frac{R_o}{R_o - R_s - b_{st}}\right)} \tag{A.1.8}$$

■ *Length and surface RS_{14}*

$$l_{S14} = h_{s1} + h_{sy} \tag{A.1.9}$$

$$S_{S14} = \frac{2\pi}{p}\alpha\left((R_o - b_s - b_{st})^2 - (R_o - b_s - 2b_{st})^2\right) \tag{A.1.10}$$

■ *Length and surface RS_{15}*

$$l_{S15} = \left(\left(R_o - \frac{3}{2}b_{st} - b_s\right) - \left(R_i + \frac{w_{st}}{2}\right)\right)\cos\gamma \tag{A.1.11}$$

$$S_{S15} = \frac{2\pi}{p}\alpha\left(R_o - b_s - \frac{3}{2}b_{st}\right)b_{st} \tag{A.1.12}$$

■ *Length and surface RS_{16}*

$$l_{S16} = h_{st} \tag{A.1.13}$$

$$S_{S16} = \frac{2\pi}{p}\alpha\left((R_i + w_{st})^2 - R_i^2\right) \tag{A1.14}$$

(2) Reluctance of the second element of the stator: R_{S2}

In the same way, the total reluctance of the second stator is the sum of all stator portions as follows:

$$R_{S2} = R_{S21} + R_{S22} + R_{S23} + R_{S24} + R_{S25} + R_{S26} \tag{A.2.1}$$

■ *Length and surface RS_{21}*

$$R_{S21} = \frac{l_{S21}}{\mu_0 \mu_{r21}(B) S_{S21}} \tag{A.2.2}$$

where

$$l_{S21} = h_{st} \tag{A.2.3}$$

$$S_{S21} = \frac{2\pi}{p}\alpha\left(R_o^2 - (R_o - w_{st})^2\right) \tag{A.2.4}$$

■ *Length and surface RS_{22}*

$$l_{S22} = h_S - \frac{1}{2}h_{sy} - h_{st} \tag{A.2.5}$$

$$S_{S22} = \frac{2\pi}{p}\alpha\left(R_i + \frac{b_{st}}{2}\right)b_{st} \tag{A.2.6}$$

■ *Length and surface RS_{23}*

$$l_{S23} = b_{st} + b_s \tag{A.2.7}$$

$$S_{S23} = \frac{2\pi}{p}\alpha h_{sy}\frac{b_{st} + b_s}{\ln\left(\frac{R_i + b_s + b_{st}}{R_i + \frac{b_{st}}{2}}\right)} \tag{A.2.8}$$

■ *Length and surface RS_{24}*

$$l_{S24} = h_s + \frac{1}{2}h_{sy} \tag{A.2.9}$$

$$S_{S24} = \frac{2\pi}{p}\alpha b_{st}\left(R_i + b_s + \frac{3}{2}b_{st}\right) \tag{A.2.10}$$

■ *Length and surface RS_{25}*

$$l_{S25} = h_s - h_{st} - \frac{1}{2}h_{sy} \tag{A.2.11}$$

$$S_{S25} = \frac{2\pi}{p}\alpha\left((R_i + b_{st})^2 - R_i^2\right) \tag{A.2.12}$$

■ *Length and surface RS_{26}*

$$l_{S26} = h_{st} \tag{A.2.13}$$

$$S_{S26} = \frac{2\pi}{p}\alpha\left((R_i + w_{st})^2 - R_i^2\right) \tag{A.2.14}$$

(3) Reluctance of the PMs: R_{PM}

The permanent magnets of the A-TFPMSM have two PM groups, the first group is outer and second inner. The sections are different as shown in Figure 18.

- Reluctance of PM_1

$$R_{01} = \frac{L_{PM1}}{\mu_0 \mu_{rPM} S_{PM1}} \tag{A.3.1}$$

where

$$L_{PM1} = h_{PM} \tag{A.3.2}$$

$$S_{PM1} = \tau_p \left(R_o^2 - (R_o - l_m)^2\right) - \theta_f \left(R_o^2 - (R_o - l_m)^2\right) \tag{A.3.3}$$

- *Reluctance of PM_2*

$$L_{PM2} = h_{PM} \tag{A.3.4}$$

$$S_{PM2} = \alpha \left((R_i + l_m)^2 - R_i^2\right) \tag{A.3.5}$$

(4) Reluctance of the rotor

Rotor reluctances consist of normal and tangential components.

- In the normal direction

$$R_{rn} = \frac{l_{rn}}{\mu_0 \mu_{rr}(B) S_{rn}} \tag{A.4.1}$$

where

$$l_{rn} = R_o - R_i - l_m \tag{A.4.2}$$

$$S_{rn} = \frac{2\pi}{p} \frac{h_r (R_o - R_i - l_m)}{\ln\left(\frac{R_o}{R_i}\right)} \tag{A.4.3}$$

- In the tangential direction
  - ■ Reluctance rotor for outer diameter

$$l_{rt1} = \frac{(R_i + l_m/2)}{2} \frac{2\pi}{p} \tag{A.4.4}$$

$$S_{rt1} = h_r \left(\frac{R_o - R_i}{2}\right) \tag{A.4.5}$$

  - ■ Reluctance rotor for inner diameter

$$l_{rt2} = \frac{(R_o - l_m/2)}{2} \frac{2\pi}{p} \tag{A.4.6}$$

$$S_{rt2} = S_{rt1} \tag{A.4.7}$$

(5) Leakage reluctances

Similar to the rotor yoke, the leakage reluctances have two components:

(5–1). The total leakage in the tangential direction (outer diameter) is done by:

$$R_{Lt1} = R_{mmt1} + R_{mgt1} + R_{cct1} \tag{A.5.1}$$

where: R_{mmt1}, R_{mgt1} and R_{cct1} are the magnet to magnet neighbor, magnet to core, and core to core, respectively.

- The magnet to magnet leakage reluctance R_{mmt1}

$$R_{mmt1} = \frac{\pi}{\mu_0 l_m \ln\left(1 + \frac{\pi g}{\tau_1}\right)} \tag{A.5.2}$$

where

$$\tau_1 = \theta_f \left(R_o - \frac{l_m}{2}\right) \tag{A.5.3}$$

- The magnet to stator core leakage reluctance R_{mgt1}

$$R_{mgt1} = \frac{4 l_{mgt1}}{\mu_0 S_{mgt1}} \tag{A.5.4}$$

where

$$l_{mgt1} = \pi \frac{h_{PM}}{2} \tag{A.5.5}$$

$$S_{mgt1} = \alpha \frac{2\pi}{2} \left(R_o - \frac{l_m}{2}\right) h_{PM} \tag{A.5.6}$$

- The magnet to stator core leakage reluctance R_{cct1}

$$R_{cct1} = \frac{l_{cct1}}{\mu_0 S_{cct1}} \tag{A.5.7}$$

where

$$l_{cct1} = \theta_f \left(R_i - \frac{l_m}{2}\right) \tag{A.5.8}$$

$$S_{cct1} = w_{st} h_{st} + b_{st} h \tag{A.5.9}$$

(5–2). The total leakage in the tangential direction (inner diameter) is done by:

$$R_{Lt2} = R_{mmt2} + R_{mgt2} + R_{cct2} \tag{A.5.10}$$

- The magnet to magnet leakage reluctance R_{mmt2}

$$R_{mmt2} = \frac{\pi}{\mu_0 l_m \ln\left(1 + \frac{\pi g}{\tau_2}\right)} \tag{A.5.11}$$

where

$$\tau_2 = \theta_f \left(R_i + \frac{l_m}{2}\right) \tag{A.5.12}$$

- The magnet to stator core leakage reluctance R_{mgt1}

$$R_{mgt1} = \frac{4 l_{mgt1}}{\mu_0 S_{mgt1}} \tag{A.5.13}$$

where

$$l_{mgt2} = \pi \frac{h_{PM}}{2} \tag{A.5.14}$$

$$S_{mgt2} = \alpha \frac{2\pi}{2} \left(R_i + \frac{l_m}{2}\right) h_{PM} \tag{A.5.15}$$

- The magnet to stator core leakage reluctance R_{cct1}

$$R_{cct2} = \frac{l_{cct2}}{\mu_0 S_{cct2}} \tag{A.5.16}$$

$$l_{cct2} = \theta_f \left(R_i + \frac{l_m}{2}\right) \tag{A.5.17}$$

$$S_{cct2} = w_{st} h_{st} \tag{A.5.18}$$

(5–3) the leakage of PM

- Leakage magnet: R_{LPM1}

$$R_{LPM1} = \frac{h_m}{\mu_o \theta_f \left(R_o - \frac{l_m}{2}\right) l_m} \tag{A.5.19}$$

- Leakage magnet: R_{LPM2}

$$R_{LPM2} = \frac{h_m}{\mu_0 \theta_f \left(R_i + \frac{l_m}{2}\right) l_m} \tag{A.5.20}$$

6) Air-gap reluctances

$$R_{gap1} = \frac{l_{gap}}{\mu_0 S_{gap1}} \tag{A.6.1}$$

$$R_{gap2} = \frac{l_{gap}}{\mu_0 S_{gap2}} \tag{A.6.2}$$

$$R_{gap} = \frac{\left(R_{gap1} + R_{gap2}\right)}{2} \tag{A.6.3}$$

$l_{gap\,=\,g}$: The air-gap reluctance of each divided elements.

S_{gap}: Air-gap areas that are perpendicular to the air-gap flux path of every divided elements constants.

APPENDIX 2

The constants in Eq. (6) are calculated as follows:

$$R_1 = R_{rt1} + 2R_{eq2} + \frac{R_{eq2}}{R_{rn}} R_{rt1} \tag{A2.1}$$

$$R_2 = \frac{R_{eq2}}{R_{rn}} R_{rt2} \tag{A2.2}$$

$$R_3 = \frac{R_{eq1} R_{rt1}}{R_{rn} R_1} \tag{A2.3}$$

$$R_4 = 2R_{eq1} + \frac{R_{eq1} R_{rt2}}{R_{rn}} - R_2 R_3 + \left(1 + \frac{R_{eq1}}{R_{rn}}\right) \tag{A2.4}$$

$$R_5 = \left(\frac{R_{rt1}}{R_1}\right)\left(\frac{R_{eq1}}{2R_{rn}} + \frac{R_{eq2}}{R_{rt1}} + \frac{R_{eq2}}{2R_{rn}} + \frac{1}{2}\right) \tag{A2.5}$$

$$R_6 = \frac{R_{eq1} R_{rt2}}{2R_{rn}} + \frac{R_{eq2} R_{rt2}}{2R_{rn}} + \frac{1}{2} R_{rt2} \tag{A2.6}$$

$$R_7 = \frac{R_{rt1}}{R_1}\left(\frac{R_{eq1}}{2R_{rn}} + \frac{R_{eq2}}{R_{rt1}} + \frac{R_{eq2}}{2R_{rn}} + \frac{1}{2}\right) \tag{A2.7}$$

$$R_8 = R_{eq1} + \frac{R_{eq1} R_{rt2}}{2R_{rn}} + \frac{R_{eq2} R_{rt2}}{2R_{rn}} + \frac{1}{2} R_{rt2} \tag{A2.8}$$

$$R_9 = \frac{R_{g1} R_{rn}}{R_{Ln}} + \frac{2R_{rn} R_5 R_2 R_3}{R_{Ln} R_4} \tag{A2.9}$$

$$R_{10} = \left(\frac{R_6 R_3}{R_4}\right)\left(1 + \frac{2R_{rn}}{R_{Ln}}\right) - \left(\frac{R_3 R_2}{R_4}\right)\left(3 + \frac{2R_{rn}}{R_{Ln}}\right) R_5 \tag{A2.10}$$

$$R_{11} = R_5\left(1 - \frac{R_2}{R_4}(1 - R_3)\right) + \frac{R_6}{R_4}(1 - R_3) - 1 \tag{A2.11}$$

$$R_{12} = 1 - R_7\left(1 - \frac{R_2}{R_4}\right) - \frac{R_8}{R_4}(1 - R_3) \tag{A2.12}$$

$$R_{13} = R_7\left(\frac{R_2}{R_4} - \frac{2R_{rn}}{R_{Ln}} - 1\right) + \frac{R_8}{R_4}\left(R_3 - \frac{2R_{rn}}{R_{Ln}}\right) \tag{A2.13}$$

$$R_{14} = \frac{R_{g1} 2R_{rn} R_2 R_7}{R_{Ln} R_4} + \frac{R_8 2R_{rn}}{R_4 R_{Ln}} + R_{g2} \tag{A2.14}$$

BIOGRAPHIES

Mohamed el Hadi Bendib received the BSc and MSc degrees in electrical engineering from Setif University and Batna University, Algeria, in 2006 and 2011, respectively, and he is a Ph.D member of the LAS Laboratory, University of Setif 1. He is currently working in National High School of Electrical Engineering and Energetic, Oran, Algeria as an associate professor. His research interests are in the electrical machine design, renewable energy, and electrical drives.

Mabrouk Hachemi was born in Setif (Algeria), on May 08, 1955. He received his degree in electrical engineering from the University of Oran (Algeria) in 1981 and the master's degree in electrical engineering from the University of Setif (Algeria). He received his PhD degree from the University of Setif (Algeria) in Electrical Engineering in 2007. He is currently a professor at the Department of Electrical Engineering, University of Setif. His main research interests are analysis, simulation and design of electrical machines, energy storage systems, and renewable energy.

Fabrizio Marignetti received the graduation degree with honors and the PhD degree in Electrical Engineering from the University of Naples Federico II in 1993 and in 1998, respectively. In 1998, he joined the University of Cassino, where he is currently an associate professor of power electronic converters, electrical machines, and drives. Prof. Marignetti is also the author of five patents. Since 1996 he lectures at the University of Cassino on electrical machines, electric vehicles, generators, and converters for renewable energies. Prof. Marignetti is the author and/or coauthor of more than 180 publications in his research field and five patents. Prof. Marignetti received two IEEE Prize Paper Awards in 2008 and in 2016. Dr. Marignetti received also one Prize Paper Award at the 2008 COMSOL Conference. His fields of interest are design, analysis, and digital control of electrical machines, renewable energies, and power converters.